NMR Structure of the (+)-CPI-indole/ d(GACTAATTGAC)-d(GTCAATTAGTC) Covalent Complex**

Carla Bassarello,[a] Paola Cimino,[a] Giuseppe Bifulco,[a] Dale L. Boger,[b] Jarrod A. Smith,[c] Walter J. Chazin,[c] and Luigi Gomez-Paloma*[a]

We report the NMR solution structure of (+)-CPI-indole (CPI, 1,2,8,8a-tetrahydrocyclopropa[c]pyrrolo[3,2-e]indol-4(5H)-one), an agent belonging to the CC-1065/duocarmycin family of antitumor compounds. This (+)-CPI-indole structure is covalently bound to d(G_1ACTAATTGTC$_{11}$)-d(G_{12}TCAATTAGTC$_{22}$), a synthetic DNA duplex containing a high-affinity binding site. The three-dimensional structure has been determined by several cycles of restrained molecular dynamics calculations with a total of 563 NMR-derived constraints, both in vacuo and by using the generalized Born solvent continuum model. In-depth analysis of the structure of this ligand–DNA complex led to a detailed knowledge of the bound state conformation of the CPI-indole, the most simplified agent related to CC-1065 and duocarmycins, the parent members of a family of extremely potent antitumor compounds. Comparison of the CPI-indole bound conformation with those previously found for (+)-duocarmycin SA (DSA), its unnatural enantiomer (−)-DSA, and the demethoxylated analogue (+)-DSI in their DNA complexes provided additional evidence of the tight correlation between the catalytic effect exerted by DNA on the alkylation reaction and the extent of angular twist between the two planar heteroaromatic subunits of these agents. Additionally, comparison of the structural features of the DNA-bound state of a "naked" ligand, such as CPI-indole, with those of various other duocarmycin agents provided useful information for the interpretation of the observed effects on chemical reactivity of the different substitution patterns at the hemispheres of these types of complex.

Introduction

Although the role of RNA in the catalysis of (bio)chemical processes has been known for over 20 years, it is only recently that the catalytic activity of nucleic acids entirely composed of DNA has been investigated. Such molecules, sometimes referred to as DNAzymes, have been obtained by in vitro selection and combine the catalytic activity of the ribozymes with the well-known chemical stability of oligodeoxynucleotides. Interesting developments in this field include DNAzymes able to cleave target RNA sequences[1, 2] and DNA-based biosensors for metal ions.[3] Another example of DNA catalysis is the role of AT-rich duplex DNA in accelerating the adenine alkylation rate of many compounds belonging to the CC-1065 and duocarmycin family of antitumor antibiotics, in a suicide enzymatic reaction.[4] The parent compound, (+)-CC-1065 (**1**), was first isolated in 1978 from cultures of *Streptomyces zelensis* and *Streptomyces* C-329.[5] Since then, many chemical and biological investigations of this class of molecules have been reported, not only for their exceptional in vitro and in vivo anticancer activities,[6–11] but also resulting from their unique mechanism of action.[12]

One of the most intriguing chemical features of these agents is their stability under a variety of solvolytic conditions, despite their spiro-cyclopropyl ring system. This property is in stark contrast to their very efficient alkylation of DNA, which occurs through cyclopropyl ring opening upon nucleophilic attack of the N3 atom of an adenine residue. This reaction occurs rapidly when a CC-1065/duocarmycin compound is exposed to appropriate sequences of duplex DNA. Two main models have been proposed to explain the observed DNA catalytic effect: the

[a] *Prof. L. Gomez-Paloma, Dr. C. Bassarello, Dr. P. Cimino, Dr. G. Bifulco*
Dipartimento di Scienze Farmaceutiche
Università degli Studi di Salerno
84084 Fisciano, Salerno (Italy)
Fax: (+39) 89-962828
E-mail: gomez@unisa.it

[b] *Prof. D. L. Boger*
Department of Chemistry
and The Skaggs Research Institute for Chemical Biology
The Scripps Research Institute
10550 North Torrey Pines Road
92037 La Jolla, California (USA)

[c] *Dr. J. A. Smith, Prof. W. J. Chazin*
Center for Structural Biology
Vanderbilt University
5142 BIOSCI/Medical Research Building III
Nashville, Tennessee 37232-8725 (USA)

[**] *CPI = 1,2,8,8a-tetrahydrocyclopropa[c]pyrrolo[3,2-e]indol-4(5H)-one*

 © 2003 Wiley-VCH Verlag GmbH & Co. KGaA, Weinheim DOI: 10.1002/cbic.200300642

alkylation site model and the noncovalent induced twist model.[13] The alkylation site model assumes inherently different abilities of various DNA sequences to protonate the C6 carbonyl group of the cyclohexadienone ring (in the alkylating subunit) and thus increase the electrophylic character of the cyclopropyl ring. The noncovalent induced twist model explains the unique DNA alkylating properties of duocarmycins as resulting from alterations in critical intersubunit angles that occur upon binding to AT-rich duplex DNA and vastly increase the electrophilicity of the cyclopropyl ring. Thus, the strict conformational and steric requirements imposed by the narrow and deep minor grooves of AT-rich DNA sequences are accommodated by an alteration in the conformation of the ligand. This conformational change leads to a reduction in the coplanarity of the two subunits (described by the three torsion angles χ_1, χ_2, χ_3, see Scheme 1)

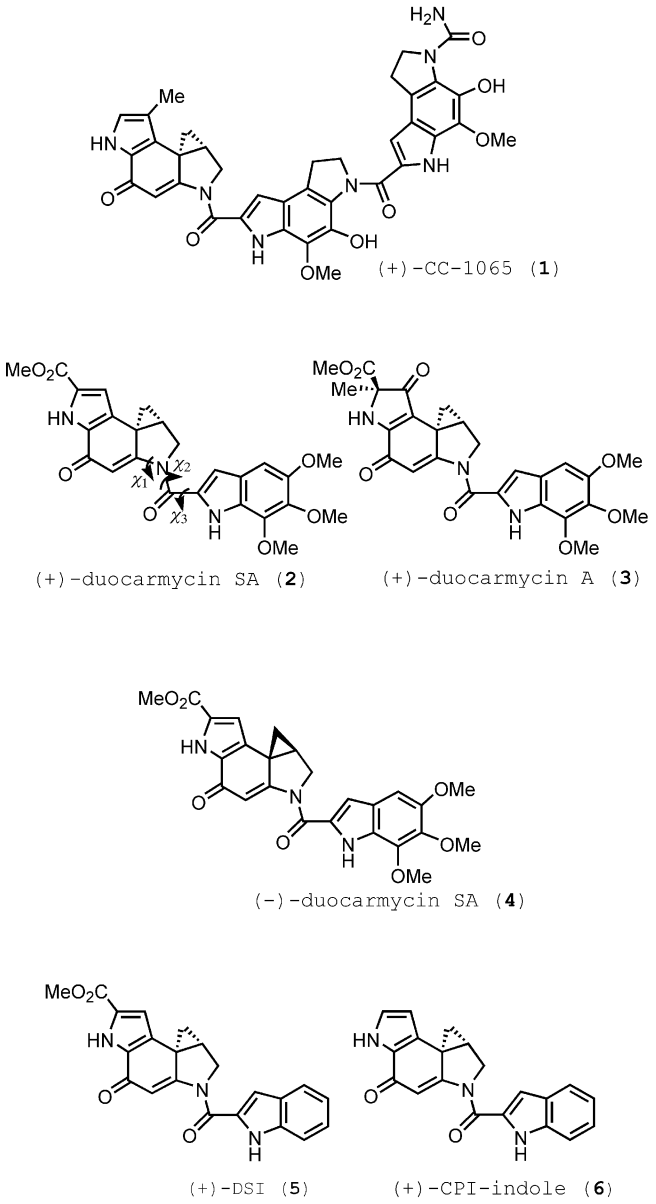

*Scheme 1. Structures of (+)-CC-1065 (**1**), (+)-duocarmycin SA (**2**), (+)-duocarmycin A (**3**), (−)-duocarmycin SA (**4**), (+)-DSI (**5**), and (+)-CPI-indole (**6**). The torsion angles χ_1, χ_2, and χ_3 are indicated on **2**.*

and thereby disrupts the high degree of conjugation present in the ground state that confers high stability to the cyclopropyl ring. Although there is a wealth of experimental and theoretical data that support this view,[14–16] direct and conclusive evidence requires detailed knowledge of the potential energy reaction profile of the DNA alkylation reaction and ultimately of the geometry and energetics of the transition state.[17]

Useful insights into the structural basis of the in situ activation of duocarmycin SA have been derived from three high-resolution NMR structures of 1:1 complexes of (+)-DSA (**3**), (−)-DSA (**4**), and (+)-DSI (**5**) all bound to d(GACTAATTGAC)-d(GTCAATTAGTC).[18–20] These results led to the hypothesis that the in situ activation of duocarmycin ligands toward DNA alkylation depends upon the extent of intersubunit twist. A three-way correlation was observed between: a) the steric hindrance induced by substituents on either subunit that extend the length of the molecule; b) the extent of intersubunit twist of the ligand in the DNA complex; and c) the rate of DNA alkylation. We proposed that conformational changes in the ligand precede the formation of the covalent bond between the adenine N3 atom and the cyclopropyl methylene carbon atom.[21] The binding-induced conformational change and accompanying activation for the subsequent DNA alkylation reaction would be a direct consequence of the adaptation of its three-dimensional shape necessary to fit the DNA minor groove. This implies that the energetic cost of activation is compensated for by noncovalent binding to DNA.[22]

The three structural studies of DSA – DNA complexes allowed the examination of structure–activity relationships involving substituents at the edge of the binding subunit and the stereochemistry of the cyclopropyl ring. The effect of substitutents at the edge of the alkylation subunit has not been structurally characterized. The effect of the methoxy groups on the binding subunit has been examined previously. We have structurally characterized the covalent complex obtained with the simplest DSA alkylating agent because it serves as the most appropriate reference for the covalent complexes (Scheme 2). Accordingly, the complex between d(GACTAATTGAC)-d(GTCAATTAGTC) and (+)-CPI-indole (**6**) was prepared, and its high-resolution solution structure was determined by using the previously described in vacuo protocols and a new protocol incorporating a continuum solvent model for aqueous media and following the Generalized Born approximation.[23–25]

Results and Discussion

^{1}H NMR characterization of the adduct

The general strategies for sequence-specific assignment of the ^{1}H resonances of small DNA duplexes are well established. Accordingly, the specific protocols used in the study described herein for chemical shift assignments on the free and bound DNA species are only briefly summarized. In particular, all cytosine 5H-6H and thymine 5Me-6H resonances were readily identified by scalar connectivities in 2Q, PE-COSY, and TOCSY spectra. All 22 discrete 1′H-2′H-2′′H-3′H-4′H-5′H-5′′H spin subsystems were identified in the 2Q, PE-COSY, and TOCSY spectra

 © 2003 Wiley-VCH Verlag GmbH & Co. KGaA, Weinheim

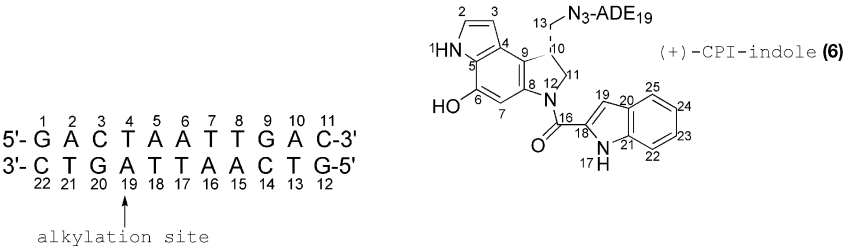

*Scheme 2. Schematic representation of (+)-CPI-indole (**6**) bound to A19 of the DNA duplex. Sequence and numbering of the 11mer DNA duplex (left) and of **6** (right) used in this study.*

and were confirmed by inspection of the NOESY spectra. The sequential resonance assignments were obtained from the NOESY spectra (see Table S1 in the Supporting Information).[26, 27] The pattern of chemical shift differences between the bound and free DNA species ($\Delta\delta_{\text{bound-free}}$) indicated that in the DNA complex, the (+)-CPI-indole (CPII) molecule is bound in the expected location within the recognition site (AATTA, see Figure S1 in the Supporting Information). Like the previously studied DSA adducts, the alkylation of the AATTA duplex occurs at the N3 position of A19 (Scheme 2 and Figure 1).

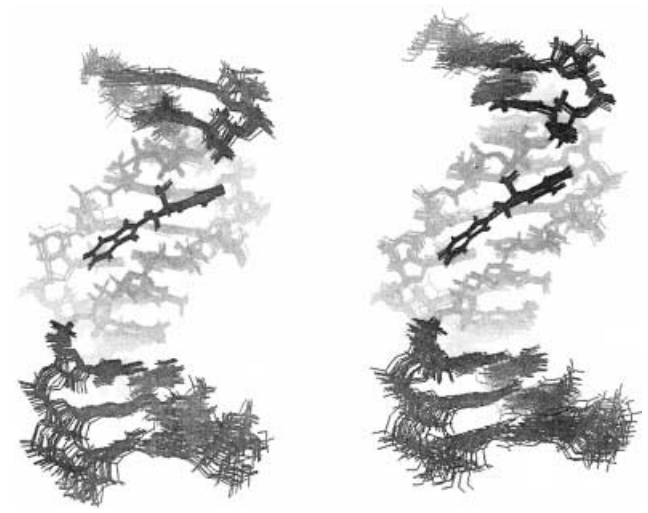

Figure 1. 3D structure of the conformational ensemble calculated in vacuo (left) and with the GB solvent continuum model (right). The model represents the covalent complex of CPII and the duplex containing the AATTA site. The 20 least-violated structures are superimposed by fitting to all atoms in the binding site (the CPII molecule and base pairs 3G·C20 – T8·A15).

Three-dimensional structure of the adduct

The intrinsic stability of the covalent complex is reflected in the relatively large number of structural constraints that can be derived from the NMR spectra. This high number of constraints in turn provides high accuracy and precision in the three-dimensional structure of the (+)-CPII – DNA complex. A total of 563 experimental constraints were identified, including 397 distances, 151 dihedral angles, and 15 Watson – Crick hydrogen bonds. The distribution of intraresidue (240), interresidue (104), and intermolecular (53) constraints is shown in Figure S2 in the Supporting Information. An average of 24 constraints per residue were obtained, with 34 per residue in the critical binding site region. Forty initial structures, generated by the NAB program,[28] were individually refined with the final input constraints by using the SANDER module of the AMBER software.[29] A total of 20 structures were selected on the basis of lowest constraint violation energies to represent the final in vacuo ensemble (Figure 1). These structures were then subjected to a further round of calculations to investigate the effect of a more sophisticated treatment of electrostatic interactions and solvation. For this purpose, the final simulations included the Generalized Born (GB) approximation, where the solvent is implicitly represented as a continuum with the dielectric properties of water.[23, 24] Table 1 reports the statistics for the structures obtained in vacuo and using the GB solvent model. Both ensembles of structures are characterized by low constraint violation energies and low values of root mean square deviations (RMSDs), which suggests that the two ensembles of structures have a high level of precision and accuracy. Differences between the two sets of structures are slight, especially in the critical AATTA binding site (the mean pairwise RMSD between the in vacuo and GB structures for the binding site region is 1.17 Å). This result is a reflection of the very

Table 1. Structural statistics for the final ensembles of the (+)-CPII – DNA complex.

Average AMBER energies [kcal mol^{-1}] Violation statistics RMSD statistics [Å][a]	
In Vacuo	
E_{total}	-1627 ± 5
Distance violations > 0.38 Å	0
40 starting DNA structures	3.04
$E_{\text{Lennard-Jones}}$	-394 ± 5
PPA violations > 7.0°	0
20 final structures: all atoms	0.89 (0.62)
$E_{\text{distance violation}}$	5 ± 2
Average bond deviation from ideal [Å]	0.007
20 final structures: binding site[b]	0.77 (0.53)
$E_{\text{torsion violation}}$	2.4 ± 0.3
Average angle deviation from ideal [deg.]	2.5
GB model	
E_{total}	-4562 ± 5
Distance constraint violations > 0.25 Å	0
20 final structures: all atoms	0.87 (0.60)
$E_{\text{Lennard-Jones}}$	-424 ± 3
Torsion constraint violations > 10.4°	0
20 final structures: binding site[b]	0.73 (0.51)
$E_{\text{distance violation}}$	5 ± 1
Average bond deviation from ideal (Å)	0.01
$E_{\text{torsion violation}}$	1.9 ± 0.2
Average angle deviation from ideal (deg.)	2.6

[a] Mean pairwise RMSD between the structures. RMSD from the mean structure is given in parentheses. [b] Binding site region includes residues C3 to T8, A15 to G20, and the entire (+)-CPI-indole molecule.

 © 2003 Wiley-VCH Verlag GmbH & Co. KGaA, Weinheim

large number of experimental data that define this structure. The only substantial difference between the two ensembles is the representation of the frayed ends of the DNA duplex, which are not well defined by the experimental data. This observation has been attributed to differences in the sampling properties of the in vacuo and GB simulations and does not greatly affect the conclusions reached in this study.[23–25]

Analysis of structural features of the DNA

The most accurate assessment of the structural features of the complex is obtained by averaging over the ensemble of the structures.[30] The observed values of the pseudorotational angle *P*, describing the deoxyribose ring puckering, are in a range that is indicative of a C2′-*endo* conformation domain, which suggests a variation around the C2′-*endo* and C1′-*exo* conformations characteristic of a regular B-DNA helix. Only the two terminal residues adopt the O4′-*endo* conformation. It is noteworthy that A19 (the alkylation site) and G20 adopt the C2′-*endo* conformation. The DNA backbone torsion angles indicate a standard B-DNA conformation, except for some residues in the vinicity of the covalent bond to CPI. The values of γ (33°), ε (-83°), and ξ (150°) at A19 are remarkably different from the average values (60°, 69°, and 90°, respectively) for all other residues. This behavior seems to be associated with the necessity to compensate for alkylation of A19 by shifting toward the major groove.

In this complex, there is a reorientation of the A19 base with regard to the deoxyribose ring and a perturbation of the A5–T18 base pair (see Supporting Information). Interestingly, the C3–G20 base pair does not exhibit the perturbations previously observed for the (+)-DSA and (+)-DSI-adducts, nor is an unusual twist at the base pair T4–A19 observed. The compression and stiffness of base pairs A6–T17 and T7–A16 in the (+)-DSI–DNA adduct shifts in the CPI-indole adduct to the base pair T8–A15, which has a twist of 40°. A perturbation in the stacking of base pairs T4–A19 and A5–T18 is also evident, as reflected in the noncanonical values of buckle, propeller twist, and rise (see the Supporting Information). All of the differences found between this adduct and the adducts of (+)-DSA and (+)-DSI can be related to the greater simplicity of the CPII structure, for example, the absence of bulky substituents at the outer edges of both subunits. There is a clear continuation of the general trend from more-substituted (DSA) to simpler ligands (DSI and CPII), in which the DNA minor groove in the binding site is broader in proportion to the effective length of the molecule. Thus, the presence of functional groups at the outer edge of both subunits contributed to expansion of the DNA minor groove.

There are some small but significant differences between the structures calculated in vacuo and with the GB model. Although overall the DNA binding sites are very similar, the GB structures exhibit a narrower minor groove width (Figure 2). This observation may be the result of superior modeling of electrostatic screening resulting from the solvent, because the negatively charged backbones are in close proximity within the narrow minor groove in AT-rich sequences.

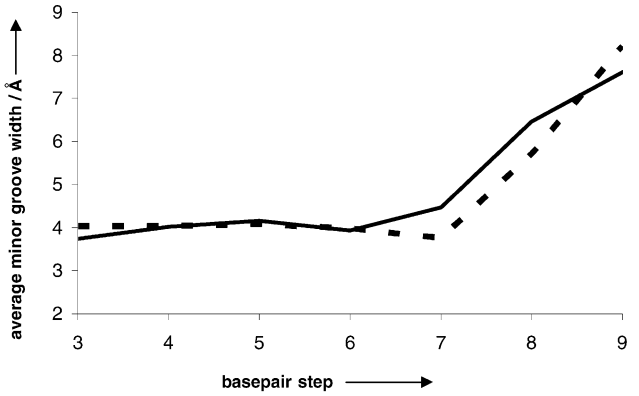

Figure 2. *Plot of the average minor groove width for the base pairs (C3·G20–G9·C14) of the covalent complexes calculated in vacuo (solid line) and with the GB solvent continuum model (dashed line).*

Analysis of structural features of the ligand

The absence of the bulky methoxy groups on the binding subunit and the lack of methyl ester on the alkylation subunit seem to enable the ligand to penetrate more deeply into the DNA minor groove. The average χ_1, χ_2, and χ_3 torsion angle values are 14.2 ± 1.1, 14.7 ± 1.2, and 8.8 ± 1.2°, respectively. Intriguingly, these numbers are very similar to the values 14.2 ± 0.3, 13.4 ± 0.6, 9.7 ± 1.0° in the (+)-DSI–DNA adduct (Table 2). On the basis of the observed difference in alkylation rates between CPII and DSI, one could expect a more visible influence on the amount of intersubunit twist found in the bound conformation of the two ligands. In fact, DNA alkylation kinetics data for AT-rich duplexes shows that CPII is about 10-fold less reactive than (+)-DSI ($k_{CPI}/k_{DSA} \sim 0.004$; $k_{DSI}/k_{DSA} \sim 0.05$).[31] Thus, either the intersubunit twist is not sufficient as the sole indicator of reactivity or the methyl ester on the alkylating subunit has a different effect (it must have some effect–the efficiency is 10× different for CPII and DSI) that modulates the alkylation efficiencies of these agents.

Table 2. *Comparison of three torsional angles χ_1, χ_2, χ_3 and of the intertwist $\chi_1+\chi_2+\chi_3$ for the various covalent adducts.*

Ligand–DNA Complex	χ_1	χ_2	χ_3	Total Twist ($\chi_1+\chi_2+\chi_3$)	RMSD from the mean [Å]
(+)-DSA	22.4 ± 0.5	11.0 ± 0.3	11.4 ± 2.0	44.8 ± 2.8	0.54
(+)-DSI	14.2 ± 0.3	13.4 ± 0.6	9.7 ± 1.0	37.3 ± 1.9	0.57
(+)-CPII (in vacuo)	14.2 ± 1.1	14.7 ± 1.2	8.8 ± 1.2	37.5 ± 1.4	0.62
(+)-CPII (GB model)	17.0 ± 2.2	17.4 ± 1.5	5.4 ± 1.3	39.7 ± 2.7	0.60
(−)-DSA	11.2 ± 1.2	4.5 ± 0.4	5.4 ± 1.0	21.2 ± 2.6	0.40

 © 2003 Wiley-VCH Verlag GmbH & Co. KGaA, Weinheim

The electronic nature of the pyrrole ring substitution has a significant effect on reactivity. Under solvolytic conditions at pH 3, DSA and CPI-indole lifetimes are 177 h and 27 h, respectively, which implies that the DSA molecule, characterized by a greater degree of conjugation at the alkylating subunit, is 6–7 times more stable than the naked CPI-indole agent.[31] This pattern inverts in the presence of DNA, where DSA is a more effective DNA alkylating agent than CPII. In such conditions, the removal of an electron withdrawing group with hydrogen acceptor properties, such as the DSA methyl ester, may account for the diminished DNA alkylation efficiency (as a result of the increase of the rigid length of the agent), perhaps accompanied by a decreased DNA noncovalent affinity.

Comparison of the 3D structure of the CPII–DNA adduct in with that of the DSI–DNA adduct reveals several subtle differences in the location and arrangement of the two agents in the DNA minor groove that may explain the differential chemical properties of these molecules. The (+)-CPII binding unit is located deeper in the groove than the (+)-DSI adduct. This difference is reflected in the average distances of the ligand atoms H19, H24, and H25 from atoms of the A_5-T_{18}, A_6-T_7, and T_7-A_{16} base pairs.[32] The offset in the orientation of the binding subunit is a direct consequence of a different orientation of the alkylating subunit, which in turn results from the absence of hydrogen bonding interaction between the G_{20} amino group protruding in the minor groove and the carbonyl oxygen atom of the C2 methyl ester group (present in DSI and absent in CPII; Figure 3). Although the CPII alkylating subunit is more exposed to the solvent than (+)-DSI, (+)-CPII is somewhat more twisted than would be expected. The unexpectedly large twist is correlated with a significantly deeper penetration of both subunits into the minor groove. Interestingly, the width of the DNA minor groove in the vicinity of the T_4-A_{19}, A_5-T_{18}, and T_7-A_{16} base pairs is smaller for the CPI-indole adduct (bp step: **4**, 4.01 ± 0.19; **5**, 4.16 ± 0.12; **6**, 3.93 ± 0.21; **7**, 4.47 ± 0.42) than for the DSI adduct (bp step: **4**, 4.46 ± 0.21; **5**, 4.72 ± 0.24; **6**, 3.64 ± 0.15; **7**, 5.74 ± 0.39). This structural feature of the DNA is probably induced by the positioning of the CPI-indole binding subunit deep in the DNA minor groove, driven by stronger van der Waals interactions of the binding subunit with the DNA cavity. Differences in the pattern of NMR-derived constraints found for the various duocarmycin agents would also be consistent with this view. For instance, while in the case of the DSA–DNA complex NOESY spectra do not show any close contacts between the drug H19 and H25 (lying in the binding subunit) and DNA protons, strong drug–DNA dipolar effects arising from the same protons are observed for the CPII–DNA complex. In this context, the pattern of DSI–DNA H19–H25 NOESY contacts is consistent with the intermediate level of minor-groove penetration of the binding subunit of DSI with respect to that of DSA and CPII (see Figure 3).

In conclusion, a comparative structural analysis of DNA adducts of CPII with those of other DSA analogues suggests that the methyl ester on the alkylation subunit may have an effect on the reactivity that goes beyond its mere ability to increase the rigid length of the molecule. The ability of the methyl ester to form hydrogen bonds with the DNA is certainly another crucial factor.

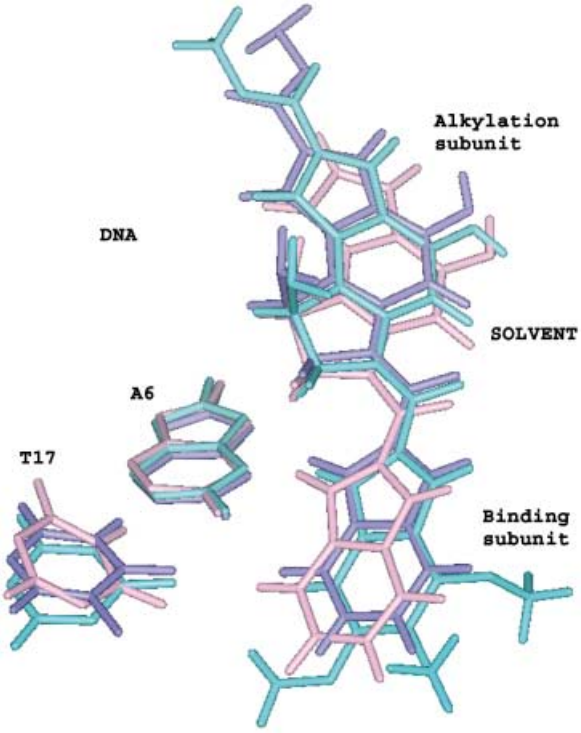

Figure 3. Differences in the relative penetration of (+)-DSA (green), (+)-DSI (blue), and (+)-CPI-indole (pink) into the DNA minor groove.

Experimental Section

Sample preparation: The purified d(GTCTAATTGAC) and d(GTCAATTAGAC) DNA oligomers were purchased from Sigma Genosys (London, England). To assess site selectivity and optimal conditions for the full-scale reaction, several analytical-scale reactions were carried out and monitored by HPLC. The reaction produced one major product, indicating the same site selectivity as observed for (+)-DSA and (+)-DSI. For the preparation of the final NMR sample, the duplex (1 μmol) was incubated with (+)-CPII (1.4 μmol) for 16 h at 310 K in a buffer at pH 7 (7.5 mM K_2HPO_4/KH_2PO_4 and 7.5 mM KCl). The reaction was monitored by HPLC and ^1H NMR spectroscopy showed that the alkylated duplex did not require any purification. The sample was lyophilized, dissolved in D_2O (450 μL), and placed in an NMR tube. The excess of ligand precipitated and was left at the bottom of the tube. Two NOESY experiments were carried out after the sample was back-exchanged in H_2O/D_2O (9:1) for the chemical shift assignments of exchangeable protons.

NMR experiments: NMR experiments were performed on a Bruker DRX-600 at 300 K. Three scalar-correlated spectra were acquired: 2Q ($\tau_e = 30$ ms, 96 scans/t_1 value, $t_{1max} = 53$ ms), P.E.COSY (35° observation pulse, 16 scans/t_1 value, $t_{1max} = 100$ ms), TOCSY spectra ($\tau_{mix} = 120$ ms, 120 scans/t_1 value, $t_{1max} = 76$ ms). Three NOESY spectra in D_2O were acquired at with $\tau_{mix} = 50$, 70, 200 ms, 16 scans/t_1 value, and $t_{1max} = 53$ ms. Two NOESY spectra in H_2O/D_2O (9:1) with $\tau_{mix} = 50$ and 200 ms (64 scans/t_1 value, $t_{1max} = 42$ and 18 ms, respectively) were acquired at 300 K using a watergate sequence to suppress the water ^1H signal. All data were processed on a Silicon Graphics Indigo2 workstation using Felix 95 software (Biosym Technologies, Inc., San Diego, CA).

 © 2003 Wiley-VCH Verlag GmbH & Co. KGaA, Weinheim

Experimental constraints: Loose dihedral constraints on the DNA backbone angles β, γ, χ, and ε were obtained from the methods described by Reid and co-workers.[33] These were combined with the pseudorotation (P) constraints obtained by fitting the Karplus equations describing the torsions of the deoxyribose ring to data obtained from the P.E.COSY experiment. Quantitative measurements of $^3J_{H1'-H2'}$ and $^3J_{H1'-H2''}$, were combined with qualitative measurements of $^3J_{H3'-H4'}$, $^3J_{H2'-H3'}$, and $^3J_{H2''-H3'}$ collected in the 2Q spectra, to determine the final allowed range of P.

Distance constraints were obtained by converting the NOE intensities that were measured in the 50 ms D_2O NOESY and in the 200 ms H_2O NOESY spectrum (for the exchangeable protons) using a two-spin approximation with multiple calibration points. The upper bounds derived from the NOE intensities at 50 ms and an additional margin of 1.0 Å were added to compensate for errors.[18] In the final stages of the calculations, the upper bounds were re-defined using MARDIGRAS hybrid relaxation matrix calculations.[34] All lower bounds were set to the sum of the van der Waals radii, that is, 1.8 Å.

Watson – Crick hydrogen bonds were enforced for all imino and amino groups whose ^{1}H resonances could be assigned, using distance constraints on the corresponding N N or N O distance involved.[35]

Structure calculations: The observation of characteristic NOEs and ^{1}H-^{1}H coupling constants indicated that the DNA duplex occupied a right-handed helical conformation (e.g., A-form, B-form). Thus, the first structure refinement was carried out on the DNA alone, beginning with a family of 40 widely varied DNA starting models of right-handed helical duplexes (RMSD = 3.04 Å) constructed with Nucleic Acid Builder (NAB)[28]. This refinement was carried out by using the restrained molecular dynamics simulated annealing (rMDSA) protocol. Arbitrarily selected values of x-displacement, incline, twist, and rise were utilized. Additional structure refinement continued with a restrained molecular dynamics docking (rMDD) of (+)-CPI-indole onto the DNA, and two rounds of rMDSA on the complex. Each starting structure was refined with 20 ps of rMDSA (1 ps of heating to 1000 K, 4 ps of high-temperature dynamics, and gradual cooling back to 0 K over the final 15 ps; RMSD = 2.52 Å). Starting structures for rMDD were generated by randomly pairing each refined DNA structure with a structure of (+)-CPI-indole derived from a restrained molecular dynamics simulation of the agent alone. The ligand was placed 10 Å outside the minor groove in the proper orientation of binding as determined from qualitative analysis of intermolecular NOEs. The automated docking was then carried out using 30 ps of rMD during which the DNA-DNA and the (+)-CPII-DNA constraint weighting was ramped on from 0.005 to 0.05 during the first 5 ps, from 0.05 to 0.2 during the following 5 ps, from 0.2 to 1.0 during the next 10 ps, and kept at 1.0 for the remaining 10 ps of computation (pairwise all-atom RMSD = 1.62 Å). The resulting docked structures of the intact complex were then refined with two successive rounds of 20 ps rMDSA as described above (pairwise all-atom RMSD = 1.44 Å).

Molecular dynamics simulations were performed in vacuo with the SANDER module of the AMBER simulation and modeling package. A constant distance-dependent dielectric was used, and phosphate charges were reduced to 20% of their full value to compensate for the lack of solvent screening effects. All in vacuo calculations were carried out on a SGI Indigo2 equipped with an R10000 processor.

The final in vacuo structures were then used as input structures for refinements using the GB model. For this purpose, 1 or 2 rounds of 20 ps rMDSA were performed using AMBER-'94 force field parameters and full charges on all phosphate groups under the Generalized-Born solvent approximation continuum model. This model has shown to be particularly suitable for the description of the electrostatic properties of biomacromolecules in aqueous environments.[23–25] In our case, the solvent continuum was represented by a medium with the dielectric properties of a water solution containing a total salt concentration of 0.2 M.

Keywords: antitumor agents · DNA minor groove binding · DNA recognition · duocarmycin · NMR spectroscopy

[1] S. Santoro, G. F Joyce, *Proc. Natl. Acad. Sci. USA* **1997**, *94*, 4262 – 4266.
[2] Z. Zaborowska, J. P. Furste, V. A. Erdmann, J. Kurreck, *J. Biol. Chem.* **2002**, *277*, 40617 – 40622.
[3] J. Li, Y. Lu, *J. Am. Chem. Soc.* **2000**, *122*, 10466 – 10467.
[4] S. E. Wolkenberg, D. L. Boger, *Chem. Rev.* **2002**, *102*, 2477 – 2496.
[5] D. E. Nettleton, J. A. Bush, W. T. Bradner, US 4301248, **1982**; [*Chem. Abstr.* **1982**, *96*, 33362e].
[6] V. L. Reynolds, J. P. McGovren, L. H. Hurley, *J. Antibiot.* **1986**, *39*, 319 – 334.
[7] M. Ichimura, T. Ogawa, K. Takahashi, E. Kobayashi, I. Kawamoto, T. Yasuzawa, I. Takahashi, H. Nakano, *J. Antibiot.* **1990**, *43*, 1037 – 1038.
[8] T. Yasuzawa, Y. Saitoh, M. Ichimura, I. Takahashi, H. Sano, *J. Antibiot.* **1991**, *44*, 445 – 447.
[9] M. Ichimura, T. Ogawa, S. Katsumata, K. Takahashi, I. Takahashi, H. Nakano, *J. Antibiot.* **1991**, *44*, 1045 – 1053.
[10] M. Ichimura, T. Ogawa, K. Takahashi, A. Mihara, I. Takahashi, H. Nakano, *Oncol. Res.* **1993**, *5*, 165 – 171.
[11] W. Wrasidlo, D. S. Johnson, D. L. Boger, *Bioorg. Med. Chem. Lett.* **1994**, *4*, 631 – 636.
[12] D. L. Boger, D. S. Johnson, *Angew. Chemie* **1996**, *108*, 1542 – 1580; *Angew. Chem. Int. Ed. Engl.* **1996**, *35*, 1438 – 1474.
[13] D. L. Boger, R. M. Garbaccio, *Bioorg. Med. Chem.* **1997**, *5*, 263 – 276.
[14] D. L. Boger, R. M. Garbaccio, *J. Org. Chem.* **1999**, *64*, 5666 – 5669.
[15] D. L. Boger, A. Santillán, Jr., M. Searcey, Q. Jin, *J. Am. Chem. Soc.* **1998**, *120*, 11554 – 11557.
[16] D. L. Boger, Y. Ambroise, *Bioorg. Med. Chem. Lett.* **2002**, *12*, 303 – 306.
[17] K. N. Kirschner, M. Lee, R. C. Stanley, J. P. Bowen, *Bioorg. Med. Chem.* **2000**, *8*, 329 – 335.
[18] P. S. Eis, J. A. Smith, J. M. Rydzewski, D. A.Case, D. L. Boger, W. J. Chazin, *J. Mol. Biol.* **1997**, *272*, 237 – 252.
[19] J. A. Smith, G. Bifulco, D. A. Case, D. L. Boger, L. Gomez-Paloma, W. J. Chazin, *J. Mol. Biol.* **2000**, *300*, 1195 – 1204.
[20] J. R. Schnell, R. R. Ketchem, D. L. Boger, W. J. Chazin, *J. Am. Chem. Soc.* **1999**, *121*, 5645 – 5652.
[21] D. L. Boger, D. L. Hertzog, B. Bollinger, D. S. Johnson, H. Cai, J. Goldberg, P. Turnbull, *J. Am. Chem. Soc.* **1997**, *119*, 4977 – 4986.
[22] D. L. Boger, R. M. Garbaccio, *Acc. Chem. Res.* **1999**, *32*, 1043 – 1052.
[23] V. Tsui, D. A. Case, *J. Am. Chem. Soc.* **2000**, *122*, 2489 – 2498.
[24] J. Srinivasan, T. E. Cheatham, III, P. Cieplak, P. A. Kollman, D. A. Case, *J. Am. Chem. Soc.* **1998**, *120*, 9401 – 9409.
[25] V. Tsui, D. A. Case, *Biopolymers* **2001**, *56*, 275 – 291.
[26] J. Hartel, P. P. Lankhorst, C. Altona, *Eur. J. Biochem.* **1982**, *129*, 343 – 357.
[27] L. P. Orbons, G. A. van der Marel, J. H. van Boom, C. Altona, *J. Biomol. Struct. Dynam.* **1987**, *4*, 939 – 963.
[28] T. Macke, PhD Thesis, The Scripps Research Institute, La Jolla (USA), **1996**.
[29] D. A. Pearlman, D. A. Case, J. W. Caldwell, W. S. Ross, T. E. Cheatham, III, S. DeBolt, D. M. Ferguson, G. L. Seibel, P. Kollman, *Comp. Phys. Commun.* **1995**, *91*, 1 – 41.
[30] E. Stofer, R. Lavery, *Biopolymers* **1994**, *34*, 337 – 346.
[31] D. L. Boger, A. Santillán, Jr., M. Searcey, S. R. Brunette, S. E. Wolkenberg, M. P. Hedrick, Q. Jin, *J. Org. Chem.* **2000**, *65*, 4101 – 4111.
[32] H19-A6H2: 2.35 ± 0.04 CPII (in vacuo); 2.57 ± 0.04 DSI; H19-T7H1′: 3.44 ± 0.09 CPII (in vacuo); 3.84 ± 0.15 DSI; H19-T7H4′: 3.61 ± 0.05 CPII (in vacuo); 3.77 ± 0.10 DSI; H24-T18H5′: 3.10 ± 0.32 CPII (in vacuo); 3.89 ± 0.04 DSI; H25-T7H1′: 2.62 ± 0.08 CPII (in vacuo); 2.97 ± 0.05 DSI; H25-T18H4′: 3.14 ± 0.05 CPII (in vacuo); 3.86 ± 0.07 DSI
[33] S. G. Kim, L. J. Lin, B. R. Reid, *Biochemistry* **1992**, *31*, 3564 – 3574.
[34] B. A. Borgias, T. L. James, *J. Magn. Reson.* **1990**, *87*, 475 – 487.
[35] U. Schmitz, T. L. James, *Methods Enzymol.* **1995**, *261*, 3 – 44.

Received: April 29, 2003 [F 642]

 © 2003 Wiley-VCH Verlag GmbH & Co. KGaA, Weinheim